Influence of atmospheric pressure plasma jet processing parameters on the wettability and surface chemistry of polypropylene: relevance for adhesion phenomena

Gallant, Danick; Guégan, Johan

Publisher's version / Version de l'éditeur:

Journal of Adhesion Science and Technology, 2010-06-30

Influence of Atmospheric Pressure Plasma Jet Processing Parameters on the Wettability and Surface Chemistry of Polypropylene: Relevance for Adhesion Phenomena

Danick Gallant[1]* and Johan Guegan[2]

[1] Structural Adhesives and Corrosion Group, Aluminium Technology Centre, Industrial Materials Institute, National Research Council Canada (ATC/IMI/NRC), 501 boul. Université Est, Saguenay, Quebec, CANADA, G7H 8C3. danick.gallant@cnrc-nrc.gc.ca

[2] École Centrale de Lyon, 36 avenue Guy de Collongue, 69134 Ecully Cedex, FRANCE.

* To whom correspondence should be addressed.

Abstract

Atmospheric pressure plasma jet technology has been applied to surface treatment of polypropylene prior to its adhesive bonding to aluminium using structural adhesives. Surface modifications of polypropylene induced during plasma treatments were investigated using surface free energy measurements, attenuated total reflectance infrared spectroscopy (ATR-IR) analyses, and mechanical evaluation of epoxy and urethane bonded aluminium-polypropylene joints. On the basis of the surface free energy criterion, the influence of

parameters describing plasma treatments (i.e. primary-to-secondary gas ratios, output power source, treatment speed, plasma-to-sample distance) was determined for each gas combination employed to generate the plasma (He with O_2, N_2, CO_2, N_2O or air). By submitting polypropylene to the optimised plasma conditions defined for each gas combination, it was found using ATR-IR analyses that a complex mixture of carbonyl functionalities are induced on the surface of processed materials. Using a fitting procedure of Gaussian bands, ATR-IR spectra were resolved into single C=O stretching vibrations. It was then found that regardless of the gas mixture injected in the plasma generator, different extents of amide and COO-based chemical functions (carboxylic acids and/or esters) were introduced onto polypropylene surfaces. From the mechanical evaluation of joint strengths of adhesively bonded hybrid aluminium-polypropylene assemblies, it was generally observed that the surface chemistry induced by the plasma plays a more important role in adhesion than the surface free energy parameter. Finally, using correlations established between Owens et al. and LWAB surface free energy theories, plasma modified polypropylene surfaces were found to be basic in nature.

Keywords

Atmospheric pressure plasma jet, ATR-IR spectroscopy, polypropylene, single lap shear, surface free energy.

1. Introduction

Due to its interesting bulk properties, recyclability, low cost and lightweight, polypropylene (PP) is one of the most interesting polyolefin materials for the design of stiff aluminium-PP hybrid structures. However, the widespread use of PP (as polymer or in composites) within adhesively bonded lightweight hybrid structures is still a challenge. This situation can be explained by the low surface free energy (SFE) of PP, which makes it difficult to bond using most commercially available structural adhesives that provide durable and highly reliable aluminium-based joints (i.e. epoxy, urethane and methacrylate). From a chemical point of view, this inherent problem comes from the fact that PP, as many thermoplastic materials, is made of hydrophobic and long saturated polymer chains. Hence, to make it suitable for adhesive bonding, the surface of PP requires a pretreatment, generally oxidative, which introduces appropriate chemical polar functionalities and surface morphologies beneficial to adhesion phenomena.

Over the past 50 years, various techniques have been suggested to increase the SFE of polyolefin polymers, particularly PP. These processes, namely corona discharge [e.g., 1-8], flame treatment [e.g., 9-16], low-pressure plasmas [e.g., 17-44] and chemical-based treatments [e.g., 45-52] such as fluorination and molecular maleic anhydride grafting, are generally oxidative in nature and lead to physical and chemical modifications of the PP surface.

According to Cho et al. [53], among these pretreatments, low-pressure plasmas are generally the most efficient. However, as pointed out by Green et al. [54], results may vary depending on the processing parameters and adhesive used. Although low-pressure plasmas allow implementation of a variety of surface chemistries through the use of different reactive gases, they nevertheless present several technological and technical limitations rendering their industrial application highly improbable for most sectors. The first one arises from the fact that the vacuum chamber is restrictive in regard to the size of parts to be treated inside it. Moreover, extended exposure time (> 10 s) of the PP parts to the plasma shower were generally reported to be required to obtain satisfying surface properties in regard to adhesion [e.g., 22,23,27]. A pump-down time (e.g. 5 minutes), hold-time following plasma treatment (e.g. 1 minute) and re-pressurisation time (e.g. 10 minutes) must also be added to consider the duration of the whole plasma treatment process under low-pressure conditions, making it too slow for most manufacturing industries [54]. In order to overpass these intrinsic limitations related to the use of low-pressure plasmas, and in the aim to keep their well-known advantages (i.e. varied chemistry, highly reactive species, low temperature processes), atmospheric pressure plasma jet sources have recently been developed [55-57]. These sources present virtually no limit to the nature, shape, size and thickness of parts to be treated, because they operate at ambient pressure and are almost zero-voltage. Furthermore, their automation using a robot represents an important advantage allowing a highly efficient control of the processing parameters.

However, although evident and promising features are characterising atmospheric pressure plasma jets, there is actually no study that systematically presents the influence of plasma conditions on the introduction of PP surface modifications relevant to adhesion. Therefore, the present study will demonstrate to which extent plasma processing parameters (i.e. gas combinations and ratios, output power source, treatment speed, plasma-to-sample distance) influence the efficacy of plasma treatments performed on PP. Surface free energy measurements, based on Owens et al. and LWAB theories (overviewed in ref. 58), will also be used to quantify the wettability of plasma processed surfaces. Finally, SFE results, as well as single lap shear (SLS) strengths measured for Al-PP hybrid joints, will be correlated to the nature of chemical modifications induced on PP and resolved using attenuated total reflectance infrared (ATR-IR) spectroscopy.

2. Experimental Details

2.1. Materials

The PP substrates (monomer: CH_2=CH-CH_3) with a tensile strength of > 5400 psi and density of 0.905 were obtained from McMaster-Carr (Los Angeles, CA). Because the crystallinity of PP influences its ability to be chemically modified [59], the crystallinity percentage of the material used was evaluated from differential scanning calorimetry (DSC) measurements (DSC1 calorimeter, Mettler-Toledo, Mississauga, ON, Canada). Using a dynamic DSC run performed under a nitrogen purge at 10°C/min from 25°C to 285°C, a crystallinity percentage (α) of 59% was calculated from the ratio $\Delta H_f/\Delta H_{f100\%}$ by considering $\Delta H_{f100\%}$ = 187 J/g [60,61].

2.2. Atmospheric pressure plasma jet treatment

Plasma treatments were performed with an Atomflo™-250 plasma source from Surfx® Technologies LLC (Culver City, CA, USA). The plasma was maintained by supplying an RF excitation frequency to the electrodes. He or Ar at a 30-L/min flow rate were used as primary gases, while O_2, N_2, CO_2, N_2O and air (water-free) were used as secondary gases at flow rates ranged from 50 to 500 mL/min. Depending on the secondary gas studied, the RF power was varied from 50 to 150 W, the latter being the maximum output power deliverable by the

instrument. The AH-250C (or AH-250D) plasma torch was precisely moved over the surfaces of the materials using a six-axis Motoman 3 kg payload robot (Yaskawa Motoman, Mississauga, Canada). The plasma treatment speed ranged from 30 to 3000 cm/min, and samples were processed at a distance of 2 mm downstream of the showerhead (if not otherwise stated). Prior to the plasma treatment, PP samples were degreased using acetone with a Kimwipes™ towel.

2.3. ATR-IR spectroscopy analyses

The nature of the chemical modifications induced on the surface of PP during the atmospheric pressure plasma jet treatments was studied using attenuated total reflectance (ATR) Fourier transform infrared (IR) spectroscopy. Spectra were obtained with a Nicolet 6700 (Thermo Scientific, Madison, WI) on a horizontally mounted internal reflection element (Smart iTR™ accessory, single-reflection diamond crystal, refractive index of 2.4 at 1000 cm^{-1}, 45° angle of incidence, 128 co-added scans with a 4 cm^{-1} spectral resolution). In order to improve the detection sensitivity, a mid-IR liquid nitrogen-cooled mercury-cadmium-telluride (MCT-B) detector was used.

2.4. Surface free energy measurements

Contact angles made by various liquids on the PP surface were measured on a Krüss DSA100 drop shape analysis system (Krüss USA, Matthews, NC).

For each sample treated with the plasma jet, the SFE and its components (according to Owens et al. and LWAB theories, see ref. 58 for direct comparison of these theories) were calculated from the static contact angle of 2 µL sessile drops (average of 6 drops for each liquid) of water (γ^S = 72.80 mJ/m^2; γ^D = 21.80 mJ/m^2; γ^P = 51.00 mJ/m^2), formamide (γ^S = 58.00 mJ/m^2; γ^D = 39.00 mJ/m^2; γ^P = 19.00 mJ/m^2) and diiodomethane (γ^S = 50.80 mJ/m^2; γ^D = 50.80 mJ/m^2; γ^P = 0.00 mJ/m^2) used as probe liquids. Sufficient time was allowed for droplets to stop spreading before measuring contact angles, which were all carried out within 15 minutes after the surface treatment.

2.5. Profilometry analyses

Surface roughness characterisation of plasma treated PP substrates was performed using an optical profilometer CHR450 from STIL (Sciences et Techniques Industrielles de la Lumière, Aix en Provence, France), used in conjunction with a field chromatic optical “pen”. This instrument uses a high-resolution non-contact sensor and allows examination of opaque and/or highly reflective surface finishes. An overall z-axis resolution better than 0.03 µm is obtained.

2.6. Mechanical single lap shear (SLS) test procedure

Aluminium-PP hybrid SLS specimens were prepared according to Figure 1. The bondline thickness was 1.0 mm (0.039”) and an overlap 25 mm in length × 25 mm in width was employed. Prior to SLS specimen assembling, aluminium 6061-T6 strips were acetone degreased, abraded using an 80-grit aluminium oxide rotating pad (4” Walter Coolcut™ abrasive disc, Walter Surface Technologies, Montreal, QC, Canada) and acetone degreased again. This surface preparation was found to be sufficient to avoid any aluminium-adhesive interfacial failure. In order to investigate the compatibility of adhesives and plasma modified PP surfaces, two 2-component room-temperature curing adhesives of different chemistries were used (epoxy Loctite Hysol 9462 and urethane 3M DP-605NS). SLS specimen testing was conducted on an electromechanical MTS Alliance RT/100 test system (MTS Systems Corporation, Eden Prairie, MN, USA), equipped with a 50 kN load cell. All tests were run at a 0.5 mm/min cross-head speed, and spacers helped to align the lap shear samples in the grips to make sure the load was parallel to the adhesive layer (see Figure 1).

3. Results and discussion

3.1. Influence of plasma processing parameters on the surface free energy of polypropylene

Because the efficiency of plasma treatments is expected to be strongly dependent on the processing parameters, and in order to establish a guideline containing the whole set of optimised plasma conditions for the treatment of PP, the influence of plasma processing conditions was investigated on the basis of the SFE criterion. The Surfx Technologies Atomflo™-250 plasma instrument can be operated using two different plasma jets, because it also possesses plasma-enhanced chemical vapour deposition (PECVD) capabilities. The first model (AH-250C) is designed to be primarily employed using different mixtures of primary and secondary gases, while the second model (AH-250D) can optionally be fed with a volatile chemical precursor allowing deposition of thin organometallic or ceramic films (e.g. SiO_2, TiO_2). In a first approach, inert gases were used to study the influence of the plasma jet model on the SFE modification of PP. Inert gases are interesting for that purpose since their mild oxidising capabilities [58] are expected to highlight the relative performance of plasma heads. Moreover, inert gases such as helium and argon are known for their ability to cause crosslinking through the CASING process (Crosslinking by Activated Species of INert Gases) [62,63], which induces one of the four effects that may be observed on a surface exposed to plasma when deposition does not occur (others being surface

cleaning, ablation/etching and surface-chemical structure modification) [64-65]. Indeed, by means of CASING, carbon radicals can link to generate C-C bonds and hence a crosslinked structure is created and inhibits the hydrophobic recovery [63,66]. However, according to Okada [67] and Lyons and Dole [68], unlike polyethylene, exposure of PP to activated helium inert gas provokes as much scission as it does crosslinking. Consequently, low joint strengths are obtained with lap shear specimens. In a first series of experiments, the nature of the inert gas (helium or argon) relevant to the study of the plasma jets efficiency was determined. Using the AH-250C plasma head, following three passes at 300 cm/min of a 30-L/min He plasma operating at 80 W, an SFE of 30.9 mJ/m^2 was measured for PP (γ^D = 29.2 mJ/m^2; γ^P = 1.7 mJ/m^2). This SFE is virtually similar to the one that characterises an acetone-degreased PP material, which is 31.5 mJ/m^2 (γ^D = 30.4 mJ/m^2; γ^P = 1.1 mJ/m^2). Therefore, it appears that helium plasma does not induce surface changes to the PP that can be measured using the contact angle measurement method. However, when argon plasma treatment is performed on the PP material under exactly the same experimental conditions than those employed for the helium plasma, a significant improvement in the SFE of PP is observed for both dispersive and polar components (γ^S = 45.7 mJ/m^2; γ^D = 38.6 mJ/m^2; γ^P = 7.1 mJ/m^2). According to Bhat and Upadhyay [59], such an increase in the dispersive surface energy (30.4 $mJ/m^2 \rightarrow$ 38.6 mJ/m^2) indicates the formation of crosslinked products on the surface of PP through the occurrence of the CASING process. Notably, concerning the polar SFE component, which has been markedly increased by argon plasma treatment (1.1

$mJ/m^2 \rightarrow 7.1\ mJ/m^2$), ATR-IR spectra of PP samples have shown the presence of carbonyl functions (C=O stretching bands, 1800-1670 cm^{-1}) induced on the surface (figure not shown). Since argon by itself is not oxidative in nature, it is likely that these polar species arise from the production of reactive oxygen and/or nitrogen species through the argon plasma bombardment of the air volume located within the 2-mm gap between the plasma head and the PP sample. Also, following the pretreatment, the activated PP surface may have reacted with oxygen and/or nitrogen from ambient air. According to Lee et al. [69], surface oxidation of PP samples by argon plasma can be related to free radical and unsaturation mediated post plasma reactions. Kwon et al. [70] have demonstrated, using XPS experiments, that an atmospheric argon plasma introduces C-O, C=O and O-C=O species on the surface of PP. Therefore, because of its efficacy in modifying both dispersive and polar SFE components of a PP material, argon plasma has been chosen as the inert primary gas for comparison purposes of AH-250C and AH-250D plasma head performance.

Figure 2 presents the SFE calculated for PP as a function of argon plasma processing speed for plasma jet models AH-250C and AH-250D following a 3-pass plasma treatment of the material. For the AH-250D head, especially designed for PECVD processes, a linear decrease of the SFE is observed as the processing speed is increased ($\gamma^{S}_{(mJ/m^2)} = -0.0239V_{(cm/min)} + 56.2$; $R^2 = 0.96$). Indeed, by applying the Owens et al. theory, an SFE of 54.8 mJ/m^2 is calculated for PP processed at a speed of 30 cm/min, which is found to linearly decrease

down to 34.9 mJ/m^2 when the treatment speed is augmented to 900 cm/min. Concerning the AH-250C torch, an SFE for plasma treated PP as high as 65.2 mJ/m^2 is obtained at a 30 cm/min processing speed. However, as the treatment speed is raised, the plasma efficiency exponentially declines until an energy plateau is almost reached around 500 cm/min. Therefore, even though the efficiency of the AH-250C jet drastically diminishes as a function of the processing speed, it nevertheless presents the advantage of providing very high SFEs as long as low processing speeds are used. On the other hand, this result shows that the oxidising power delivered by the AH-250C plasma jet needs to be improved in order to operate surface treatments using a single pass in combination with a faster treatment speed. For that purpose, helium plasma was used in combination with oxygen as electronegative secondary gas. Helium is particularly interesting for mixing gases because its elevated electron temperature permits higher oxidising gas concentrations than argon [71]. At the same externally applied voltage, the electron density of argon plasma is larger than that generated in helium plasma, while the inverse trend is noticed for electron temperature. According to Ren et al. [63], excited species of helium can be generated by applying an excitation energy in the range 19.8 - 20.6 eV. Because an ionisation potential of 13.6 eV characterises oxygen molecules, a collision between a metastable helium atom and an oxygen molecule creates an ionised and highly reactive oxygen species:

$$He^* + O_2 \rightarrow O_2^+ + He + e^-$$

Figure 3 shows how oxygen addition to helium in a 1% ratio (300 mL/min O_2 + 30 L/min He) influences the SFE of PP as a function of the treatment speed. At low processing speeds (< 300 cm/min), argon plasma increases the SFE of PP more significantly than He/O_2 plasma does. At a treatment speed of 300 cm/min, the addition of 1% O_2 allows to increase the SFE of PP from 30.9 mJ/m^2 (He plasma, w/o O_2) to 44.8 mJ/m^2. A similar SFE is obtained using argon plasma without any oxygen content (45.7 mJ/m^2). However, as the processing speed is further augmented (> 300 cm/min), the efficiency of the He/O_2 plasma overpasses that of argon. Indeed, under such conditions, oxygen allows to maintain the polar component around 10 mJ/m^2. For instance, at a treatment speed of 900 cm/min, the polar component of the PP surface treated using the He/O_2 plasma is 9.6 mJ/m^2, while it is as low as 2.6 mJ/m^2 for the surface treated using argon plasma. Therefore, the addition of only 1% of O_2 as an oxidising gas to helium plasma improves the SFE of PP through a mechanism that primarily promotes the introduction of polar species within the surface polymer network, even at quite high processing speeds. The nature of chemical species responsible for the high polar SFE component will be discussed in a further section of this article.

As pointed out in Figure 4, although a high O_2:He ratio and power are used, the plasma-to-sample distance nevertheless plays a key role in the SFE modification of PP. Indeed, as the air gap between the plasma head and the PP sample was increased from 1 to 8 mm, the SFE of PP was found to importantly fall from 48.3 mJ/m^2 to 33.3 mJ/m^2. Such a trend in treatment efficiency can be

attributed to a progressive deactivation of in-flight reactive oxygen species created in the plasma shower and ultimately responsible for the introduction of polar groups on the PP surface. At a distance of 8 mm from the plasma source, almost all reactive oxygen species are deactivated and, as a consequence, $\gamma^S \approx \gamma^D$ and $\gamma^P \approx 0$. According to Li et al. [71], helium atomic mass is too low to push away ambient air and bring the generated oxygen atoms and metastable molecules farther out of the plasma jet nozzle. In the present study, a 2-mm plasma-to-sample distance was found to be adequate because of the flatness of samples. Notably, using such a plasma-to-sample distance, the surface roughness induced by etching of PP during He/O_2 plasma treatment is only significant at very low treatment speeds (i.e. 30 and 60 cm/min) (Figure 5). Moreover, because Ra values are generally low and virtually independent of the treatment speed, corrections of the SFE to account for surface roughness are useless. Green et al. [54] have demonstrated that surface topography does not play a significant role in surface adhesion of PP following a typical surface treatment that increases the O:C ratio (e.g. flame, low-pressure plasma, etc.). Therefore, surface roughness features observed on PP following most He/O_2 plasma treatments are not expected to influence PP adhesion phenomena.

In order to define optimised helium-based plasma treatment conditions, the efficiency of oxygen (O_2), nitrous oxide (N_2O), air, nitrogen (N_2) and carbon dioxide (CO_2) used as secondary gases was studied using a 1-pass plasma treatment performed at constant processing speed (300 cm/min) and plasma-to-

sample distance (2 mm). Using intermediate secondary gas flows, the influence of the plasma power on the treatment level of PP was defined. As demonstrated in Figure 6, a plasma power of 150 W allows to maximise the SFE of PP substrates except when nitrogen is used as secondary gas. It must be remembered that 150 W represents the maximum power output deliverable by the plasma generator. For the He/N_2 plasma, unstable plasma and non-reproducible treatments of PP are obtained at P > 60 W. Thus, 60 W was identified as the optimal power for the He/N_2 gas combination, which provides PP with an SFE of 44.4 mJ/m^2. Interestingly, oxidising nitrous oxide gas was found to be, by far, the secondary gas leading to the highest SFE (62.8 mJ/m^2) following only 1 pass performed at 150 W and 300 cm/min. Under the same power and processing speed, oxygen led to an SFE of 53.4 mJ/m^2. Finally, air and carbon dioxide secondary gases provided PP with a similar SFE when powered at 150 W, i.e. 46.2 mJ/m^2 and 47.3 mJ/m^2, respectively.

The influence of the secondary gas flow added to a 30-L/min helium plasma was studied at a power of 150 W for O_2, N_2O, air and CO_2, and 60 W for N_2. It is important to note that, due to limitations in the flow meter calibration, flow rates higher than 350 mL/min were not reachable with nitrous oxide and carbon dioxide. Figures 7a and 7b show the effect of the secondary gas flow on the SFE of plasma treated PP, for oxidising (i.e. O_2, N_2O and air) and non-oxidising (i.e. N_2 and CO_2) secondary gases, respectively. As shown in Figure 7a, for nitrous oxide, a flow of 100 mL/min leads to the highest SFE. Increasing the nitrous

oxide flow from 100 to 300 mL/min has a detrimental effect since the SFE varies from 62.8 to 56.7 mJ/m^2. Similarly, oxygen flows lower and higher than 300 mL/min cause a diminution of the SFE of PP. The same behaviour was observed for air, except that the optimal flow was found to be 200 mL/min. In Figure 7b, it is shown that carbon dioxide behaves like nitrous oxide since a quite low flow rate (i.e. 50 mL/min) is preferred to maximise the SFE of PP. Finally, a 350 mL/min nitrogen flow was found to provide PP with an optimised He/N_2 plasma treatment performed on it. Optimal power and flow rate determined for each secondary gas on the basis of the SFE criterion are summarised in Table 1. In a recent paper, Ren et al. [63] have discussed on the reasons why helium plasma fed with a high oxygen concentration (2%) does not activate polymers as a lower oxygen concentration (1%) does. According to Ren et al., there are two main reactions involving molecular oxygen within a plasma:

$$O_2 + e^- \rightarrow (O_2^-)_{unstable} \rightarrow O + O^- + \text{Energy}$$

$$O_2 + e^- + Y \leftrightarrow O_2^- + Y + \text{Energy}$$

where Y represents a third body (here, O_2 and/or He). At a low oxygen concentration, the formation of unstable O_2^- species is favoured and thus, atomic oxygen is mainly found as the reaction product. As the O_2 concentration is increased, interactions with the Y body become favoured and the formation of stable O_2^- species progressively occurs. However, because it has been reported that atomic oxygen plays the key role in the activation of polymer surfaces [72], an over-concentration of O_2 in the gas mixture would inhibit polymer activation. Ren et al. have also suggested that when the oxygen concentration in the

plasma increases, the O^- and atomic oxygen concentration will decrease due to increased production of ozone because it will be more likely for O^- and atomic oxygen to collide with O_2. In the case of atmospheric pressure plasma jet treatment of UHMPE, less reactive species were produced on the UHMPE surface when a large amount of oxygen was added to helium [63]. In the present research, an inhibition of the activation process has been observed for oxygen flows superior to 300 mL/min, which correspond to concentrations higher than 1% (1% O_2 = 300 mL/min O_2 per 30 L/min He). Because the SFE measured for PP samples treated with a plasma containing nitrous oxide, carbon dioxide or air also decreases at higher flow rates, it is likely that a similar third body deactivation mechanism may take place with these gases.

Using optimised plasma conditions (i.e. power and gas flow) determined for each secondary gas (see Table 1), the influence of the processing speed on the SFE of PP was studied. As presented in Figure 8, when the processing speed is augmented from 300 to 3000 cm/min, the SFE of PP treated with oxygen, carbon dioxide and air used as secondary gases slowly decreased from ~ 50-53 mJ/m^2 to ~ 40 mJ/m^2, point at which an energy plateau is nearly reached. In the case of nitrous oxide, although a rather high SFE can be obtained at a processing speed of 300 cm/min (62.8 mJ/m^2), plasma treatment efficiency also declines at high processing speeds. Finally, it was found that He/N_2 plasma treatment efficiency is drastically affected by a processing speed superior to 300 cm/min. Such behaviour can be attributed to the weak oxidising

capability expected for a low-powered He/N_2 plasma. SFEs presented in Figure 8, determined from the contact angle measured for water, formamide and diiodomethane probe liquids, have been reported in Figure 9 as a function of the inverse of the water contact angle ($1/\theta_{water}$). Notably, regardless of the gas mixture employed in the plasma, a linear relationship was found between $1/\theta_{water}$ and γ^S (or γ^P) parameters. Hence, using these relationships, each component of Owens' SFE theory can be easily quantified for a PP substrate submitted to a plasma treatment. The next section will be aimed at the resolution of surface chemistry modifications induced during the plasma treatment of PP using different gas mixtures.

3.2. ATR-IR analyses of plasma-treated polypropylene

In the aim to understand the nature as well as the extent of chemical modifications induced on the PP surface by plasma treatments, attenuated total reflectance (ATR) infrared spectroscopy (IR) analyses were performed. A diamond crystal, mounted on a single reflection accessory, was chosen to record the IR spectra of plasma treated PP samples in the carbonyl (C=O) stretching region. As presented in Figure 10, following each plasma treatment, the global absorbance growth observed in the wavenumber interval from 1850 to 1600 cm^{-1} evidences that the concentration of carbonyl species is increased on the surface of PP and, consequently, that the O:C ratio essential to adhesion [54] is improved. As seen in Figure 10, the ATR-IR spectrum recorded for PP (similar for surface and bulk) before plasma treatments indicate that chemicals incorporating C=O groups were initially present within the PP formulation, these probably being stabilising compounds (UV-absorbers, antioxidants, mould release agents, etc.) [73].

Interestingly, as shown in Figure 10, He/O_2 and He/CO_2 plasmas led to similar spectra, especially in the ester and carboxylic acid spectral region (1790-1700 cm^{-1}). Activated species O and CO, generated by a CO_2 plasma, are in fact likely to introduce COO groups within a polymer network [74]. Aouinti et al. [75] have studied the influence of CO_2 low-pressure MW plasma treatment on the SFE and surface chemistry of PP. They found, from XPS and ToF-SIMS

experiments, that alcohol, ketone and acid groups are the main functions incorporated to PP surfaces. The presence of carboxylic acid groups on PP samples treated with a CO_2 low-pressure MW plasma has also been confirmed by Médard et al. [76] from ToF-SIMS, XPS and spectrochemical titration experiments. As pointed out by Inagaki et al. [74], who compared O_2 and CO_2 low-pressure RF plasmas efficacy in modifying the surface of ETFE films, CO_2 plasma introduces a higher concentration of COO groups than O_2 plasma does. This result, evidenced from XPS experiments, is consistent with the present study since, as clearly shown in Figure 10, the highest absorbance in the carbonyl region was recorded for the PP material treated with the He/CO_2 plasma. However, at this point, ATR spectra do not allow to determine if detected COO groups belong to either carboxylic acid or ester functions or both.

As seen in Figure 10, and as expected, the ATR spectrum for the PP sample treated using He/N_2 plasma shows the lowest intensity in the COO bands region. However, Mutel et al. [77] have shown that oxygen impurities significantly modify the chemistry induced on PP samples by a N_2 plasma through the incorporation of O-rich species (R-NH_2, R-OH, C=NH, C=O, R-CO-NH_2, and O-C=O). Again, this observation is in agreement with the corresponding ATR spectrum in Figure 10 that evidences the introduction by He/N_2 plasma of complex and varied carbonyl chemistries on the PP surface. Surprisingly, in the lowest frequency interval of the carbonyl region (1700-1600 cm^{-1}), the IR absorbance recorded was found to be virtually independent of the plasma

compositions investigated. It is thus appropriate to suggest that the addition of amide functionalities to the PP surface would be the result of air ionisation located between the plasma head and PP substrate. Post plasma reactions between treated PP samples and ambient air are also likely to occur [69]. As shown in Figure 10, samples treated with an He/air plasma present absorption intensities intermediate to those observed for samples treated with He/O_2 and He/N_2 plasmas. The latter observation evidences that oxygen and nitrogen are both active in the He/air plasma. Hwang et al. [78] have recently demonstrated that He/air plasma introduces O- and N-based polar functional groups on the surface of aramid fibres.

Although both oxygen and nitrous oxide are strong oxidising gases, ATR spectra in Figure 10 show that the chemistry induced on PP by He/N_2O plasma is much closer to the chemistry generated by He/N_2 or He/air plasma than that obtained using He/O_2 plasma. One of the most interesting and distinctive features is the induction by He/N_2O plasma of nitro (NO_2) functionalities evidenced by the absorption peak located at 1558 cm^{-1}. The presence of these nitro groups would explain the relatively high SFE of PP samples treated using He/N_2O plasma, in comparison to PP samples treated using any other gas combination. Their possible role in adhesion will be discussed in the next section. In a recent paper, Strobel et al. [14] studied the influence of nitrous oxide addition to an air/natural gas flame for the pretreatment of PP. Using ESCA, they demonstrated that nitrous oxide leads to the affixation of many nitrogen-

containing chemical functional groups (e.g., $-ONO_2$, $-NO_2$, -ONO, -NO, =NOH, $-NH_2$, and ≡N) to the PP surfaces exposed to the flame. Results of this study are thus consistent with the interpretation made of ATR spectra that confirms the closeness in chemistries induced on PP by He/N_2 and He/N_2O plasmas.

In order to resolve large absorption bands characterising polymeric materials (see Figure 10), the experimental ATR-IR spectrum recorded for untreated PP was firstly decomposed according to a band fitting procedure using the minimum number of Gaussian bands. As presented in Figure 11, the three main absorption bands obtained, located at wavenumbers 1743 cm^{-1}, 1694 cm^{-1} and 1648 cm^{-1}, can be assigned to carbonyl stretching vibrations in ester, carboxylic acid and amide functional groups, respectively [79]. As mentioned before, these carbonyl bands can be attributed to additives added to bulk PP before the moulding of parts. Figure 12a and 12b present decomposed ATR spectra recorded for PP samples treated with He/O_2 and He/N_2 plasmas, respectively. Assuming that C=O groups initially present in bulk PP are not affected by plasma treatments (dotted curves), ATR spectra recorded for PP samples treated using He/O_2 and He/N_2 plasmas were decomposed (red curves), again using the minimum number of Gaussian bands. For these decomposition procedures, the same full width at half maximum (FWHM) was used for corresponding Gaussian bands in the two spectra. As shown in Figure 12, amide bands located at ~ 1635 cm^{-1} and having similar intensities are introduced by He/O_2 and He/N_2 plasma treatments, reinforcing the idea that the air gap

between the plasma torch and the sample plays a role in the surface modification of PP. On the other hand, as expected, He/O_2 plasma more importantly increases the COO concentration on the surface of PP (1790-1710 cm^{-1}) than He/N_2 plasma does. In both spectra, bands at wavenumbers ~1785 and ~1760 cm^{-1} are most likely attributable to ester groups, while the absorption band in the 1730-1710 cm^{-1} interval can be assigned to either ester or carboxylic acid groups. These three last bands are, however, clearly more intense in the case of PP treated using the He/O_2 plasma. According to Pavia et al. [79], the carbonyl stretching absorption of a carboxylic acid typically occurs at 1730-1700 cm^{-1} for the dimer and 1760-1730 cm^{-1} for the monomer. Because the corresponding stretching vibration occurs at 1750-1735 cm^{-1} in the case of esters, it becomes very difficult to differentiate acid from ester chemical functions. The fact that some conjugations may move the C=O absorption bands to lower or higher frequencies also contributes to rendering the spectral analysis more complex. It must be mentioned that relative absorption intensities observed for initially present and plasma introduced carbonyl species are not representative of the extent of surface modifications. Indeed, because the ATR technique has a depth of sampling of a few microns, and because a very thin layer (few nm [80]) of newly introduced C=O species overlays the C=O contaminated bulk PP material, the latter dominates the signature of ATR spectra.

In the aim to support the dominant presence of either carboxylic acid or ester groups on plasma treated PP materials, the SFE calculated from Owens et

al. and LWAB theories have been correlated. As presented in Figure 13a, there exists a linear relationship between the basic and the polar SFE components calculated from the LWAB and Owens et al. theories, respectively (data shown in Figure 13 originate from experimental results presented in Figure 8). For the γ^- vs. γ^P curve, the slope of 1.15, which is quite close to a 1.0 value, suggests that polar interactions would essentially come from the presence of basic species introduced on the PP surface during the plasma treatment, regardless of the plasma composition. On the other hand, as shown in Figure 13b, a very low proportion of acid species is found on PP surfaces following plasma treatments. This result points toward the idea that, in Figure 12, most absorption bands at wavenumbers higher than 1710 cm^{-1} are assignable to ester rather than carboxylic acid groups. However, because the problem pertaining to the acid/base character investigation of polymer surfaces has many times been raised in literature, further surface investigations will be required to validate results obtained from the acid-base characterisation based on contact angle measurements. Nevertheless, considering that results usually obtained from the LWAB theory are strongly dependent on the probe liquids used [e.g., 81,82], the good correlation established in Figure 13 between Owens et al. and LWAB theories makes us believe that the Owens et al. theory has provided accurate results regarding the value of dispersive and polar SFE components.

3.3. Joint strength of single lap shear aluminium-polypropylene hybrid assemblies

Figure 14 presents the joint strength of single lap shear Al-PP specimens bonded with epoxy and urethane adhesives, following the pretreatment of PP using the optimised plasma conditions defined in Table 1. As shown, when using an oxygen-containing plasma (i.e. He/O_2 and He/air plasmas), the epoxy adhesive performs better in lap shear than the urethane adhesive. This may be explained by highly compatible interactions between O-rich PP surfaces and epoxy or hydroxyl groups present in the epoxy adhesive prepolymers. However, because of the complexity of the adhesive formulation, it is almost impossible to specifically identify the component or reaction product mainly responsible for adhesion. In the case of the epoxy adhesive, more than 15 hazardous ingredients (before reticulation) are reported in the material safety datasheet of the product.

As seen in Figure 14, using He/N_2O and He/N_2 plasmas, far stronger joints are obtained with the urethane adhesive than with the epoxy resin. Again, the closeness in the chemistry of isocyanate functions (O=C=N) present in the urethane formulation with the N,O-based chemistry induced on PP by He/N_2O and He/N_2 plasmas, would explain the quite important joint strengths measured (3.53 MPa for He/N_2O and 3.83 MPa for He/N_2). This result is supported by ATR-IR spectra shown in Figure 10, which evidence that PP samples treated with

He/N_2O plasma have a chemistry much closer to the one of He/N_2 plasma treated samples than He/O_2 plasma treated parts (with the exception of the nitro group generated by He/N_2O plasma). However, on the basis of the results presented in Figure 14, it seems that nitro chemical functions introduced on PP by He/N_2O plasma do not play a key role in adhesion phenomena. It is of primary importance to mention that this result evidences the relative contributions to adhesion phenomena of surface chemistry and surface free energy concepts. Indeed, although the SFE of PP treated with an He/N_2 plasma is 16.0 mJ/m^2 lower than that measured following a treatment with the He/N_2O plasma, joint strengths are, nevertheless, slightly higher in the case of He/N_2 plasma. Consequently, the surface chemistry plays the major role in this case.

Concerning the He/air plasma, on the basis of discussed mechanical results obtained from samples treated with He/O_2 and He/N_2 plasmas, its oxygen and nitrogen content were expected to be detrimental to urethane and epoxy adhesion, respectively. In fact, consistent results were obtained since He/air plasma does not give very high joint strengths with either epoxy (2.83 MPa) or urethane (2.53 MPa) adhesives.

Finally, from the analysis of the ATR-IR spectra presented in Figure 10, it was anticipated that the He/CO_2 plasma would provide joint strengths as high as those obtained with the He/O_2 plasma. However, with the epoxy adhesive, the He/CO_2 plasma was found to be far less efficient than the He/O_2 plasma. Inagaki

et al. [74] have compared surface chemistries induced on ETFE films using both O_2 and CO_2 low-pressure plasmas. They demonstrated, using XPS experiments, that the surface compositions yielded are roughly the same for both plasmas, with the exception that the COO concentration is higher for samples treated with the CO_2 plasma. As previously mentioned, this result is consistent with the ATR spectra in Figure 10, which show a higher absorbance in the COO region for the PP sample treated using the He/CO_2 plasma. However, once again according to the Inagaki et al. study [74], lower O:C ratios are obtained with the CO_2 plasma. It is likely that the difference observed between the O:C ratio for O_2 and CO_2 plasmas arises from the fact that CO_2 introduces new carbon through CO activated species, while O_2 solely oxidises aliphatic hydrocarbon chains already present at the polymer surface. This lower O:C ratio, as well as the thinness of the surface polymer layer affected by the CO_2 plasma [74], are possible explanations to lower adhesion strengths observed for the epoxy adhesive on He/CO_2 plasma treated PP parts. Finally, up to now, we do not have any experimental evidence demonstrating that PP chain sites modified using He/O_2 and He/CO_2 plasmas are either the same or totally different. It is reasonable to suggest that this could also influence the adhesion behaviour of the plasma treated material.

4. Conclusions

The aim of this study was to investigate how relevant atmospheric pressure plasma jet is for the modification of PP prior to its adhesive bonding, especially using epoxy and urethane structural adhesives. In order to determine optimised plasma treatment conditions for each gas combination of interest, the influence of parameters characterising plasma processes was studied using SFE measurements as a validation tool. For He/O_2, CO_2, N_2O air plasmas, a power of 150 W was found to maximise the SFE of PP, while a much lower power of 60 W was the most efficient toward SFE enhancement of PP using the He/N_2 plasma. A low plasma-to-sample distance, intermediate secondary gas flows and low processing speeds were also characterising optimal plasma conditions for the treatment of flat PP surfaces. Regardless of the gas combination employed to generate the plasma, a linear relationship was observed between the inverse of contact angle made by water ($1/\theta_{water}$) and the SFE components calculated using the Owens et al. theory.

ATR-IR analyses were used to characterise, at a molecular level, the nature of surface modifications induced to PP during plasma treatments. For that purpose, the frequency interval in which carbonyl stretching vibrations occur was thoroughly studied (1850-1600 cm^{-1}). From the decomposition of ATR-IR spectra using a fitting procedure involving Gaussian bands, it was determined that plasma processes most likely introduce amide and COO-based functionalities

(esters and/or carboxylic acids). While the level of COO species introduced was found to be dependent on the gas combination employed, the amount of amide groups was found, on the other hand, to be virtually insensitive to the nature of the plasma. Such a conclusion evidences the role of ambient air in the surface chemistry modification of plasma processed PP surfaces. He/O_2 and He/CO_2 plasmas were found to introduce the highest COO concentrations on PP materials, while He/N_2 plasma was definitely the less efficient in this matter.

The mechanical evaluation of adhesively bonded aluminium-PP joints has shown that joint strengths are strongly dependent on the surface chemistry of PP, rather than subjected to SFE tendencies. Indeed, although He/N_2 plasma provides PP surfaces with the lowest SFE, it nevertheless gives the strongest aluminium-PP joints when a urethane adhesive is employed. While the He/O_2 plasma treatment is more efficient when combined to an epoxy adhesive, it was observed that PP surfaces treated with He/N_2 and He/N_2O plasmas interact more strongly with a urethane adhesive. The He/air plasma, because it contains both O_2 and N_2 that are detrimental to urethane and epoxy adhesion respectively, was not found to be efficient with either epoxy or urethane adhesives. Finally, He/CO_2 plasma treated PP parts have shown low adhesion properties, although their surface chemistry was close to the one introduced by He/O_2 plasma. Factors such as low O:C ratios and the thinness character of the surface layer modified by the He/CO_2 plasma have been suggested to explain the discrepancy between ATR-IR spectra and mechanical evaluation results. While many correlations were

successfully established between ATR-IR analyses and mechanical performance evaluations, uncertain conclusions were however obtained concerning the acid-base character of the surface discussed on the basis of ATR-IR spectra and SFE measurements. The wide range of IR absorption frequencies possibly attributable to both carboxylic acids and esters, as well as the confusion concerning the exactness of the LWAB theory in predicting the acid-base character of surfaces, explain that definitive conclusions in this regard cannot be established. Further analyses, based on ATR-IR analysis of chemically derivatised plasma treated PP surfaces, are presently under planning.

Acknowledgements

The authors wish to thank the National Research Council of Canada for its financial support.

References

1. F.P.M. Mercx, *Polymer* **34**, 1981-1983 (1993).
2. I. Novak and I. Chodak, *Angew. Makromol. Chem.* **260**, 47-51 (1998).
3. I. Novak, V. Pollak and I. Chodak, *Plasma Process. Polym.* **3**, 355-364 (2006).
4. R. Krüger and H. Potente, *J. Adhesion* **11**, 113-124 (1980).
5. I. Sutherland, R.P. Popat, D.M. Brewis and R. Calder, *J. Adhesion* **46**, 79-88 (1994).
6. J. Comyn, L. Mascia, G. Xiao and B.M. Parker, *Int. J. Adhes. Adhes.* **16**, 301-304 (1996).
7. I. Novak and S. Florian, *J. Mater. Sci.* **39**, 2033-2036 (2004).
8. M. Sira, D. Trunec, P. Stahel, V. Bursikova, Z. Navratil and J. Bursik, *J. Phys. D Appl. Phys.* **38**, 621-627 (2005).
9. M.A. Aboudzadeh, S.M. Mirabedini and M. Atai, *Int. J. Adhes. Adhes.* **27**, 519-526 (2007).
10. F. Garbassi, E. Occhiello and F. Polato, *J. Mater. Sci.* **22**, 207-212 (1987).

11. A.P. Pijpers and R.J. Meier, *J. Electron Spectrosc. Relat. Phenom.* **121**, 299-313 (2001).

12. M. Strobel, M.C. Branch, M. Ulsh, R.S. Kapaun, S. Kirk and C.S. Lyons, *J. Adhes. Sci. Technol.* **10**, 515-539 (1996).

13. I. Sutherland, D.M. Brewis, R.J. Heath and E. Sheng, *Surf. Interface Anal.* **17**, 507-510 (1991).

14. M. Strobel, N. Sullivan, M.C. Branch, J. Park, M. Ulsh, R.S. Kapaun and B. Leys, *J. Adhes. Sci. Technol.* **14**, 1243-1264 (2000).

15. M. Strobel, M. Ulsh, C. Stroud and M.C. Branch, *J. Adhes. Sci. Technol.* **20**, 1493-1505 (2006).

16. J. Park, C.S. Lyons, M. Strobel, M. Ulsh, M.I. Kinsinger and M.J. Prokosch, *J. Adhes. Sci. Technol.* **17**, 643-653 (2003).

17. M. Tatoulian, F. Arefi-Khonsari, I. Rouger-Mabille and J. Amouroux, *CIP'95 Proceedings: 10th International Colloquium on Plasma Processes*, pp. 121-125. Société Française du Vide, Antibes – Juan-Les-Pins, France (1995).

18. N. Shahidzadeh-Ahmadi, M. Tatoulian, F. Arefi-Khonsari, M.M. Chehimi and J. Amouroux, *Short and long chains at interfaces: Proceedings of the XXXth rencontres de Moriond*, pp. 325-330. Éditions Frontières, Villars sur Ollon, Switzerland (1995).

19. I.L.J. Dogué, N. Mermilliod and R. Foerch, *CIP'95 Proceedings: 10th International Colloquium on Plasma Processes*, pp. 149-152. Société Française du Vide, Antibes – Juan-Les-Pins, France (1995).

20. L. Carrino, G. Moroni and W. Polini, *J. Mater. Process. Technol.* **121**, 373-382 (2002).

21. S.L. Kaplan and P.W. Rose, *Int. J. Adhes. Adhes.* **11**, 109-113 (1991).

22. H. Gleich, R.M. Criens, H.G. Moslé and U. Leute, *Int. J. Adhes. Adhes.* **9**, 88-94 (1989).

23. T. Zeiler, S. Kellermann and H. Münstedt, *J. Adhes. Sci. Technol.* **14**, 619-634 (2000).

24. C. Mühlhan, St. Weidner, J. Friedrich and H. Nowack, *Surf. Coat. Technol.* **116-119**, 783-787 (1999).

25. S. Nowak, H.-P. Haerri, L. Schlapbach and J. Vogt, *Surf. Interface Anal.* **16**, 418-423 (1990).

26. R. Mahlberg, H.E.-M. Niemi, F. Denes and R.M. Rowell, *Int. J. Adhes. Adhes.* **18**, 283-297 (1998).

27. W. Petasch, E. Räuchle, M. Walker and P. Elsner, *Surf. Coat. Technol.* **74-75**, 682-688 (1995).

28. S. Vallon, A. Hofrichter, B. Drévillon, J.E. Klemberg-Sapieha, L. Martinu and F. Poncin-Epaillard, *Thin Solid Films* **290-291**, 68-73 (1996).

29. E. Dayss, G. Leps and J. Meinhardt, *Surf. Coat. Technol.* **116-119**, 986-990 (1999).

30. M. Tatoulian, F. Arefi-Khonsari, N. Shahidzadeh-Ahmadi and J. Amouroux, *Int. J. Adhes. Adhes.* **15**, 177-184 (1995).

31. I.L.J. Dogué, N. Mermilliod, G. Boiron and S. Staveris, *Int. J. Adhes. Adhes.* **15**, 205-210 (1995).

32. L. Carrino, W. Polini and L. Sorrentino, *J. Mater. Process. Technol.* **153-154**, 519-525 (2004).

33. K. Navaneetha Pandiyaraj, V. Selvarajan, R.R. Deshmukh and C. Gao, *Appl. Surf. Sci.* **255**, 3965-3971 (2009).

34. K. Harth and H. Hibst, *Surf. Coat. Technol.* **59**, 350-355 (1993).

35. H. Guezenoc, Y. Segui, S. Thery and K. Asfardjani, *J. Adhes. Sci. Technol.* **7**, 953-965 (1993).

36. S. Vallon, R. Brenot, A. Hofrichter, B. Drévillon, A. Gheorghiu, C. Sénémaud, J.E. Klemberg-Sapieha, L. Martinu and F. Poncin-Epaillard, *J. Adhes. Sci. Technol.* **10**, 1313-1332 (1996).

37. L. Sorrentino, L. Carrino and G. Napolitano, *Surf. Eng.* **23**, 247-252 (2007).

38. O.D. Greenwood, R.D. Boyd, J. Hopkins and J.P.S. Badyal, *J. Adhes. Sci. Technol.* **9**, 311-326 (1995).

39. F. Poncin-Epaillard, B. Chevet and J.-C. Brosse, *J. Adhes. Sci. Technol.* **8**, 455-468 (1994).

40. C. Oehr, M. Müller, B. Elkin, D. Hegemann and U. Vohrer, *Surf. Coat. Technol.* **116-119**, 25-35 (1999).

41. J.F. Friedrich, P. Rohrer, W. Saur, Th. Gross, A. Lippitz and W. Unger, *Surf. Coat. Technol.* **59**, 371-378 (1993).

42. X. Tu, R.A. Young and F. Denes, *Cellulose* **1**, 87-106 (1994).

43. S. Corn, K.P. Vora, M. Strobel and C.S. Lyons, *J. Adhes. Sci. Technol.* **5**, 239-245 (1991).

44. V. André, F. Arefi, J. Amouroux and G. Lorang, *Surf. Interface Anal.* **16**, 241-245 (1990).

45. D. Briggs, D.M. Brewis and M.B. Konieczo, *J. Mater. Sci.* **11**, 1270-1277 (1976).

46. G. Kranz, R. Lüschen, T. Gesang, V. Schlett, O.D. Hennemann and W.D. Stohrer, *Int. J. Adhes. Adhes.* **14**, 243-253 (1994).

47. C.-W. Lin, *J. Mater. Sci. Lett.* **12**, 612-614 (1993).

48. R.J. Clemens, G.N. Batts, J.E. Lawniczak, K.P. Middleton and C. Sass, *Prog. Org. Coat.* **24**, 43-54 (1994).

49. B.L. Erickson, H. Asthana and L.T. Drzal, *J. Adhes. Sci. Technol.* **11**, 1249-1267 (1997).

50. A.S. Vasconcellos, J.A.P. Oliveira and R. Baumhardt-Neto, *Eur. Polym. J.* **33**, 1731-1734 (1997).

51. F.J. du Toit and R.D. Sanderson, *J. Fluorine Chem.* **98**, 115-119 (1999).

52. M.-A. Chen, H.-Z. Li and X.-M. Zhang, *Int. J. Adhes. Adhes.* **27**, 175-187 (2007).

53. D.L. Cho, K.H. Shin, W.-J. Lee and D.-H. Kim, *J. Adhes. Sci. Technol.* **15**, 653-664 (2001).

54. M.D. Green, F.J. Guild and R.D. Adams, *Int. J. Adhes. Adhes.* **22**, 81-90 (2002).

55. J. Park, I. Henins, H.W. Herrmann, G.S. Selwyn and R.F. Hicks, *J. Appl. Phys.* **89**, 20-28 (2001).

56. X. Yang, M. Moravej, G.R. Nowling, S.E. Babayan, J. Panelon, J.P. Chang and R.F. Hicks, *Plasma Sources Sci. Technol.* **14**, 314-320 (2005).

57. X. Yang, M. Moravej, S.E. Babayan, G.R. Nowling and R.F. Hicks, *Plasma Sources Sci. Technol.* **14**, 412-418 (2005).

58. D. Gallant, *J. Adhesion* **86**, pp. To Be Determined (2010).

59. N.V. Bhat and D.J. Upadhyay, *J. Appl. Polym. Sci.* **86**, 925-936 (2002).

60. Y.I. Yun, K.S. Kim, S.-J. Uhm, B.B. Khatua, K. Cho, J.K. Kim and C.E. Park, *J. Adhes. Sci. Technol.* **18**, 1279-1291 (2004).

61. M.B. Olde Riekerink, J.G.A. Terlingen, G.H.M. Engbers and J. Feijen, *Langmuir* **15**, 4847-4856 (1999).

62. H. Schonhorn and R.H. Hansen, *J. Appl. Polym. Sci.* **11**, 1461-1474 (1967).

63. Y. Ren, C. Wang and Y. Qiu, *Surf. Coat. Technol.* **202**, 2670-2676 (2008).

64. M.J. Shenton, G.C. Stevens, N.P. Wright and X. Duan, *J. Polym. Sci. A: Polym. Chem.* **40**, 95-109 (2002).

65. E.M. Liston, L. Martinu and M.R. Wertheimer, *J. Adhes. Sci. Technol.* **7**, 1091-1127 (1993).

66. J.M. Lane and D.J. Hourston, *Prog. Org. Coat.* **21**, 269-284 (1993).

67. Y. Okada, *Adv. Chem. Ser.* **66**, 44-56 (1967).

68. B.J. Lyons and M. Dole, *J. Phys. Chem.* **68**, 526-534 (1964).

69. S.D. Lee, M. Sarmadi, F. Denes and J.L. Shohet, *Plasmas Polym.* **2**, 177-198 (1997).

70. O.-J. Kwon, S.-W. Myung, C.-S. Lee and H.-S. Choi, *J. Colloid Interface Sci.* **295**, 409-416 (2006).

71. S.-Z. Li, J.-P. Lim, J.G. Kang and H.S. Uhm, *Phys. Plasmas* **13**, 093503-1 to -7 (2006).

72. J.Y. Jeong, J. Park, I. Henins, S.E. Babayan, V.J. Tu, G.S. Selwyn, G. Ding and R.F. Hicks, *J. Phys. Chem. A* **104**, 8027-8032 (2000).

73. R. Yang, J. Tu, Y. Liu and K. Wang, *J. Appl. Polym. Sci.* **107**, 610-617 (2008).

74. N. Inagaki, K. Narushima and T. Amano, *J. Adhes. Sci. Technol.* **20**, 1443-1462 (2006).

75. M. Aouinti, P. Bertrand and F. Poncin-Epaillard, *Plasmas Polym.* **8**, 225-236 (2003).

76. M. Médard, M. Aouinti, F. Poncin-Epaillard and P. Bertrand, *Surf. Interface Anal.* **31**, 1042-1047 (2001).

77. B. Mutel, J. Grimblot, O. Dessaux and P. Goudmand, *Surf. Interface Anal.* **30**, 401-406 (2000).

78. Y.J. Hwang, Y. Qiu, C. Zhang, B. Jarrard, R. Stedeford, J. Tsai, Y.C. Park and M. McCord, *J. Adhes. Sci. Technol.* **17**, 847-860 (2003).

79. D.L. Pavia, G.M. Lampman and G.S. Kriz, *Introduction to Spectroscopy*, 2nd Ed., Chapter 2. Saunders College Publishing, Orlando (1996).

80. L.J. Gerenser, J.M. Grace, G. Apai and P.M. Thompson, *Surf. Interface Anal.* **29**, 12-22 (2000).

81. A. Holländer, *J. Colloid Interface Sci.* **169**, 493-496 (1995).

82. C. Della Volpe, D. Maniglio, M. Brugnara, S. Siboni and M. Morra, *J. Colloid Interface Sci.* **271**, 434-453 (2004).

Figures, Tables and Captions

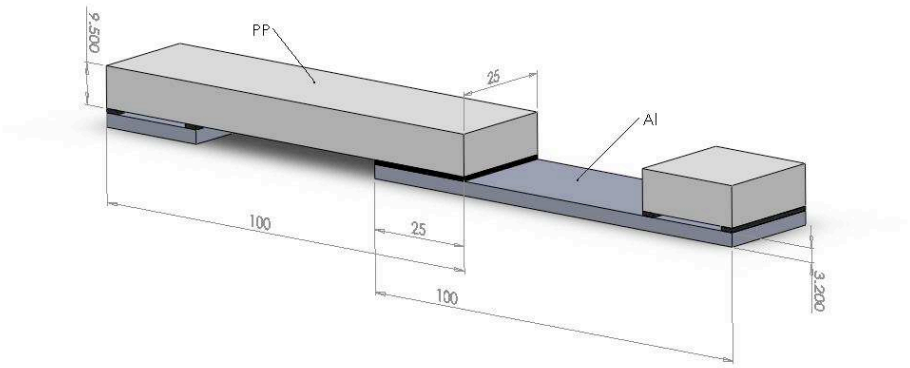

Figure 1. Hybrid aluminium-polypropylene single lap shear (SLS) specimen, all dimensions are in mm (bondline thickness: 1.0 mm).

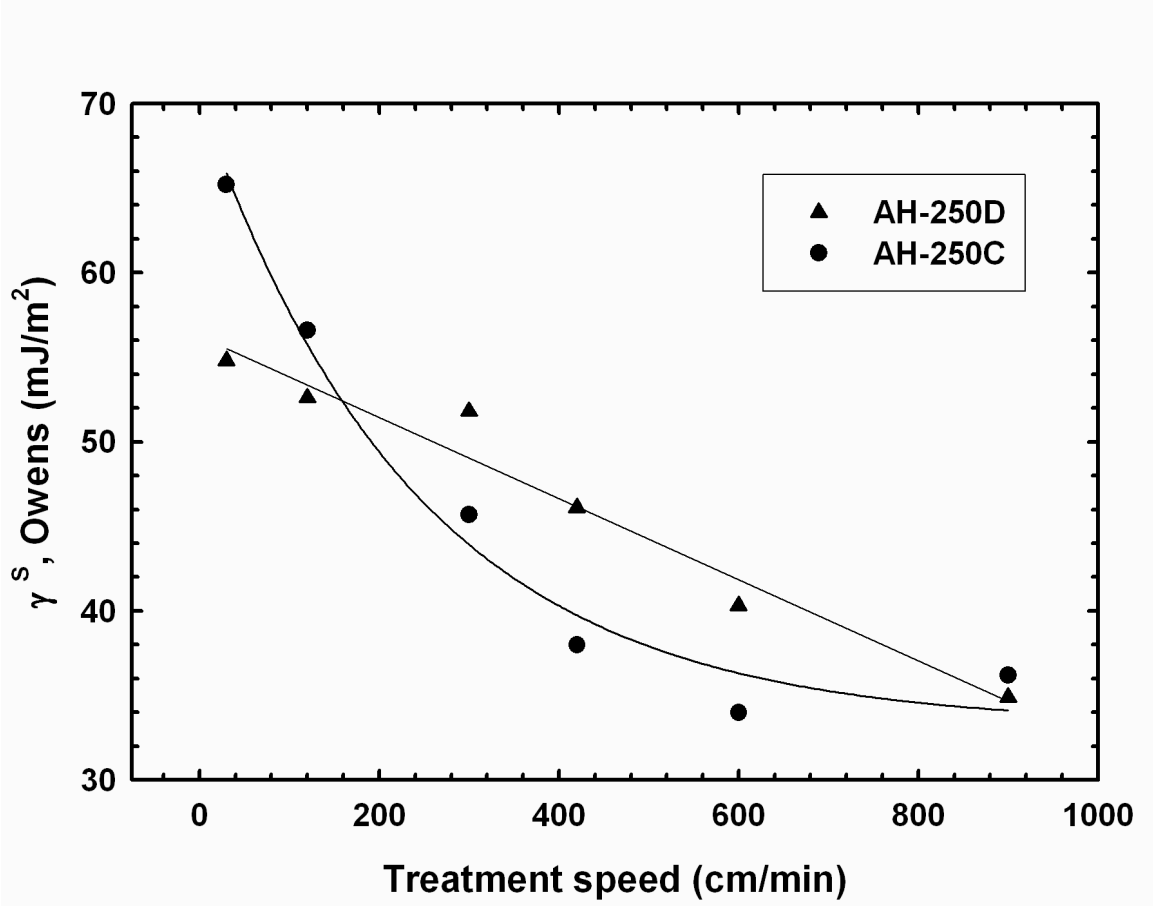

Figure 2. Influence of the plasma torch model (AH-250C, AH-250D) on the surface free energy of polypropylene treated using different plasma processing speeds (plasma treatment parameters: Ar 30 L/min, P = 80 W, 3 passes, v = 30 cm/min, plasma-to-sample distance = 2 mm).

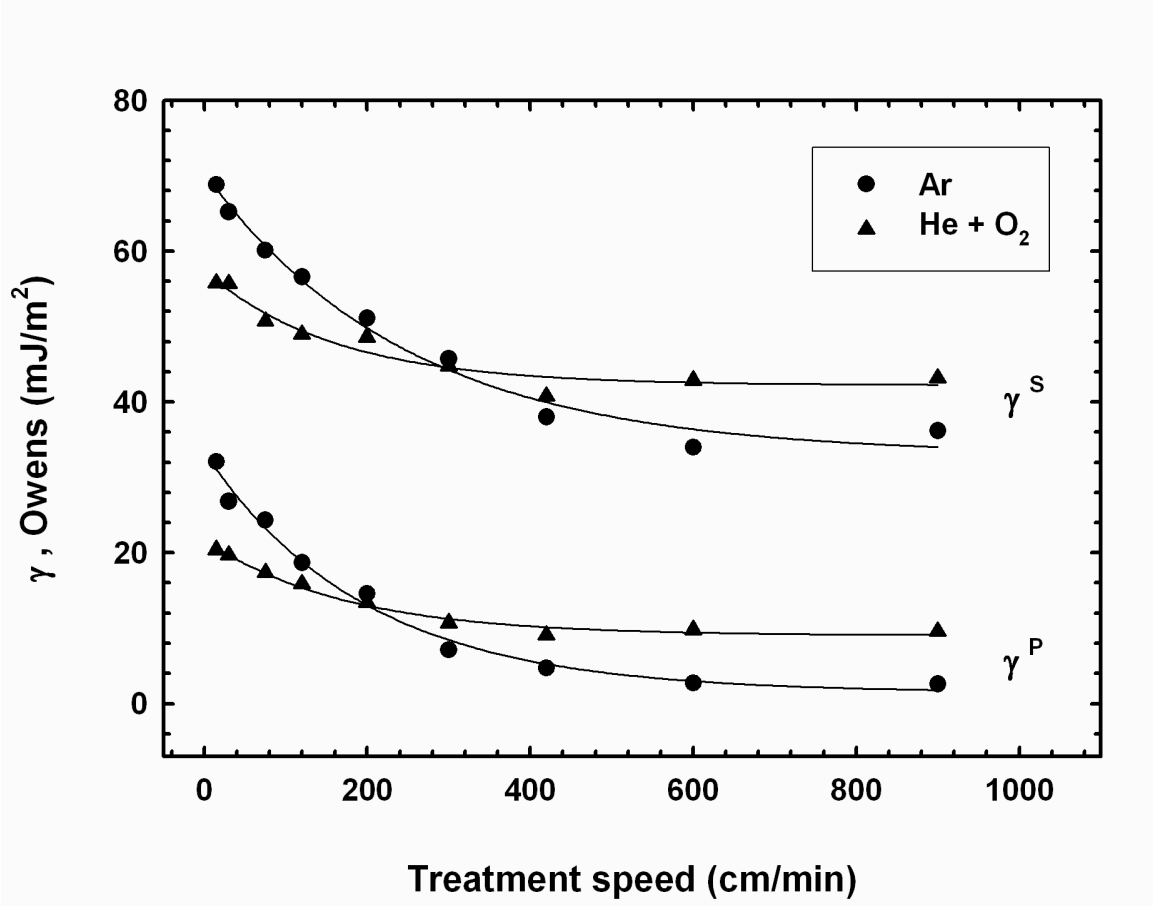

Figure 3. Effect of the secondary gas addition (O_2) on the surface free energy of polypropylene, as a function of the treatment speed (plasma treatment parameters: Ar 30 L/min, He 30 L/min + O_2 300 mL/min, P = 80 W, 3 passes, plasma-to-sample distance = 2 mm, plasma head model AH-250C).

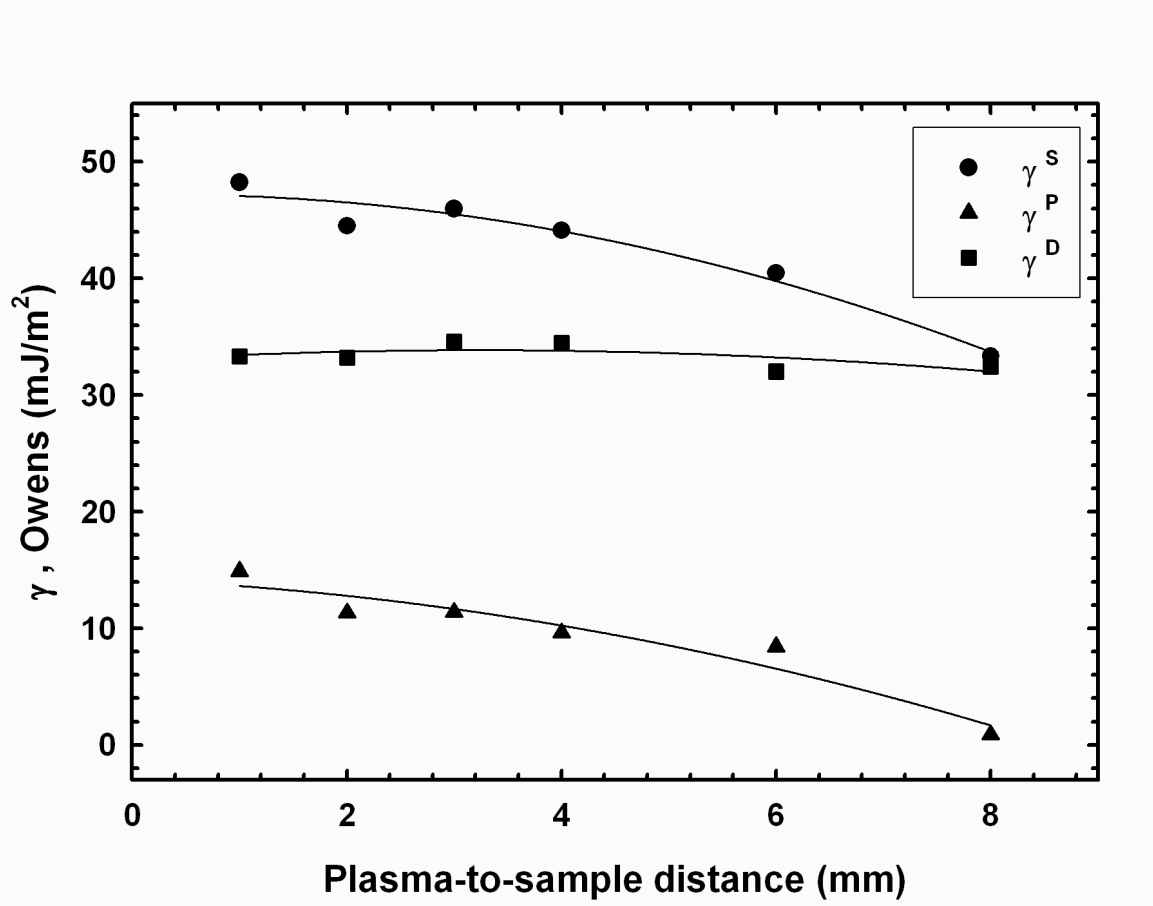

Figure 4. Influence of the plasma-to-sample distance on the surface free energy of polypropylene (plasma treatment parameters: He 30 L/min + O_2 500 mL/min, P = 150 W, 1 pass, v = 300 cm/min, plasma head model AH-250C).

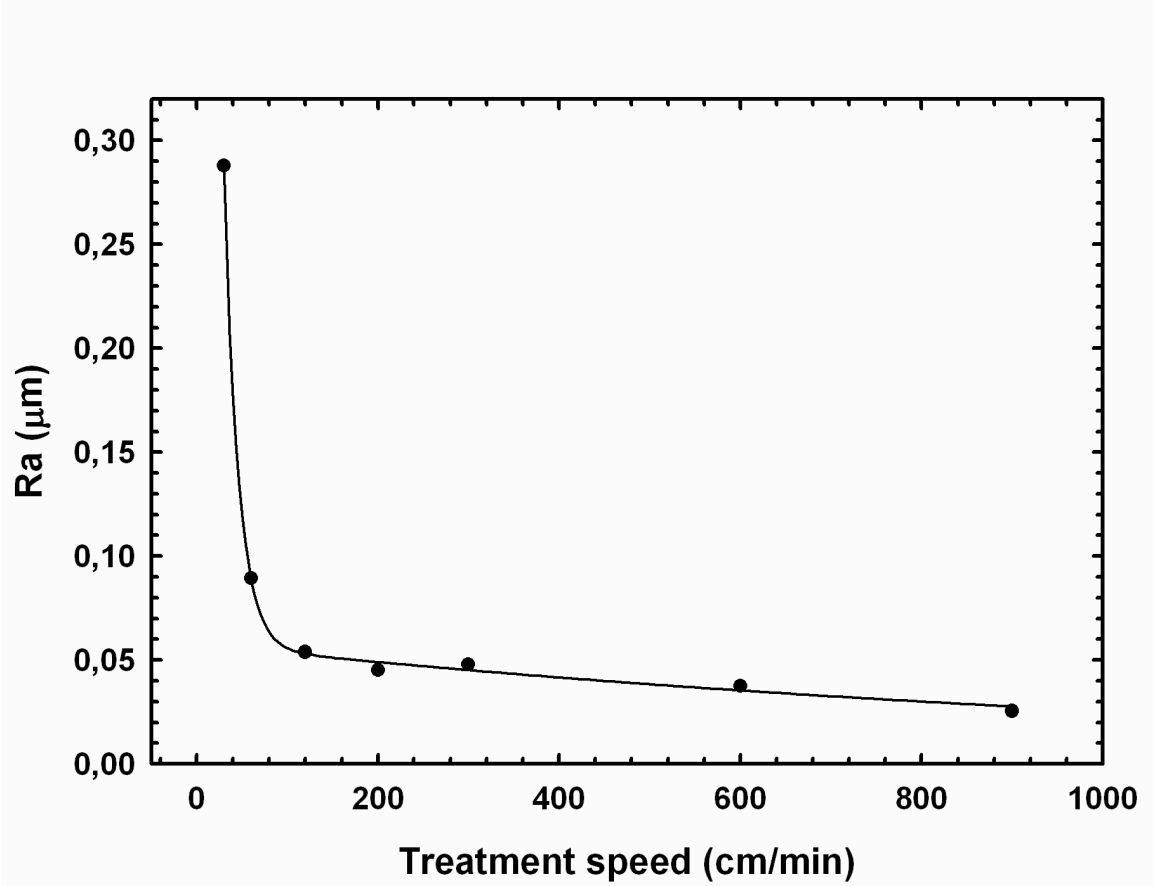

Figure 5. Influence of the plasma processing speed on the surface roughness of polypropylene (plasma treatment parameters: He 30 L/min + O_2 300 mL/min, P = 150 W, 1 pass, plasma-to-sample distance = 2 mm, plasma head model AH-250C).

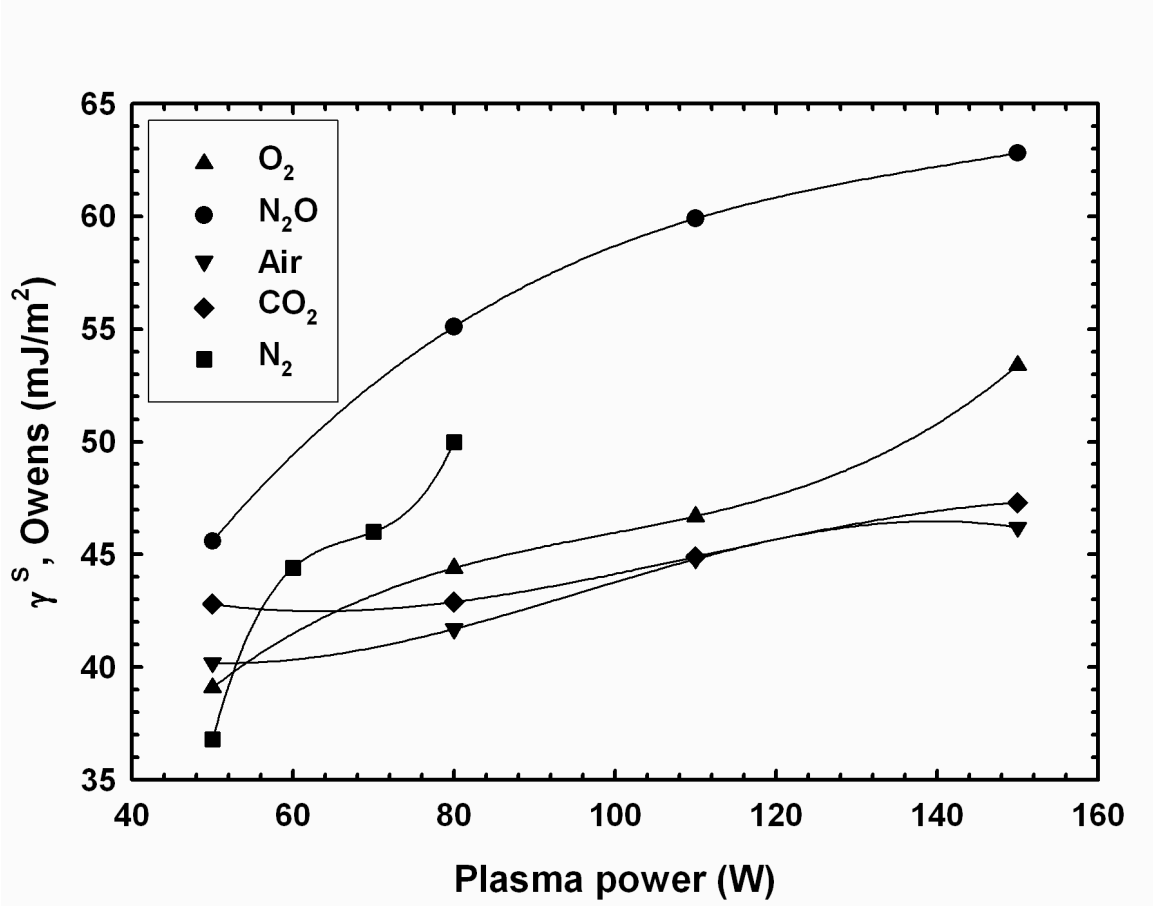

Figure 6. Influence of plasma power on the surface free energy of polypropylene treated using different He and secondary gas combinations (plasma treatment parameters: He 30 L/min + Secondary Gas = O_2 300 mL/min; N_2O 100 mL/min; Air 100 mL/min; CO_2 200 mL/min; N_2 100 mL/min, 1 pass, v = 300 cm/min, plasma-to-sample distance = 2 mm, plasma head model AH-250C).

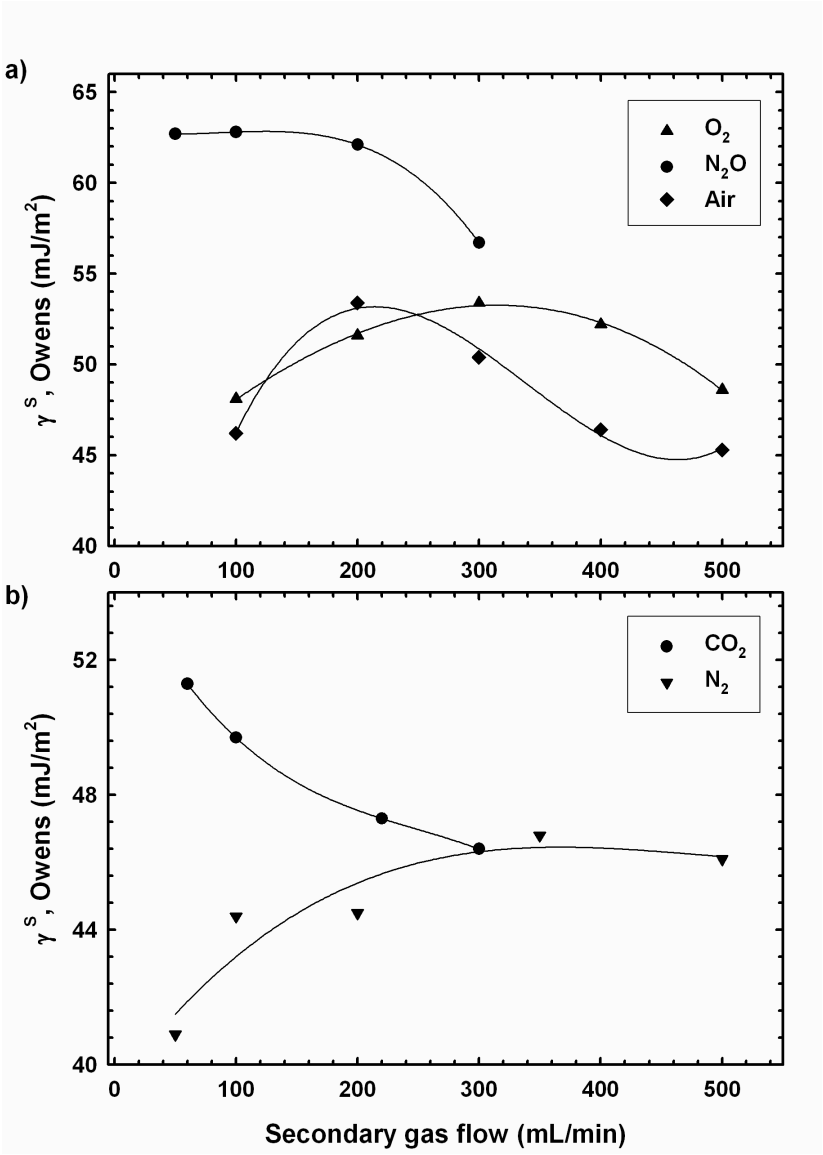

Figure 7. Effect of the secondary gas flow on the surface free energy of polypropylene treated using different mixtures of He and (a) oxidising secondary gas; (b) non-oxidising secondary gas (plasma treatment parameters: P = 150 W for He 30 L/min + O_2, N_2O, Air and CO_2, P= 60 W for He 30 L/min + N_2, 1 pass, v = 300 cm/min, plasma-to-sample distance = 2 mm, plasma head model AH-250C).

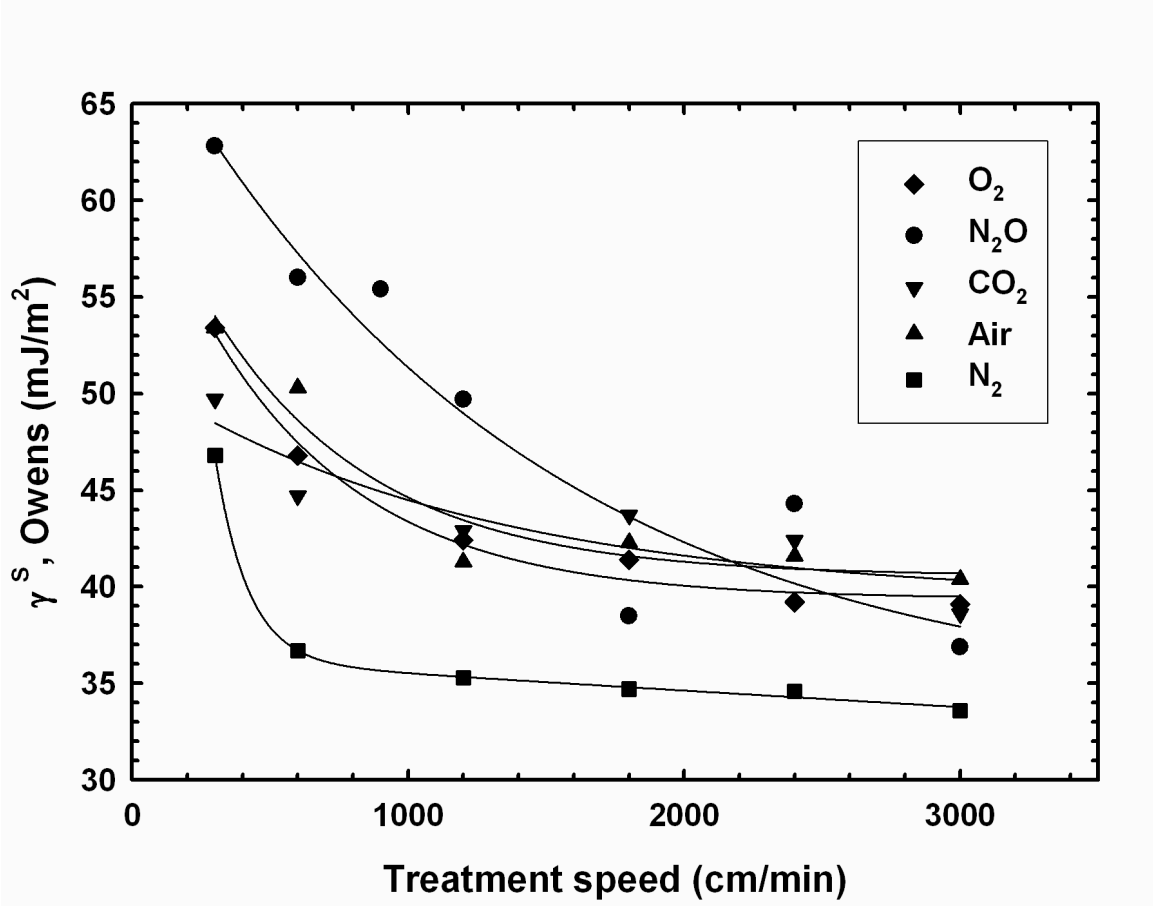

Figure 8. Influence of the treatment speed on the surface free energy of polypropylene processed using the gas ratio and output power optimised for each gas combination (plasma treatment parameters: He 30 L/min + O_2 or N_2O or CO_2 or Air or N_2, see Table 1 for power and secondary gas flow specific to each secondary gas, 1 pass, plasma-to-sample distance = 2 mm, plasma head model AH-250C).

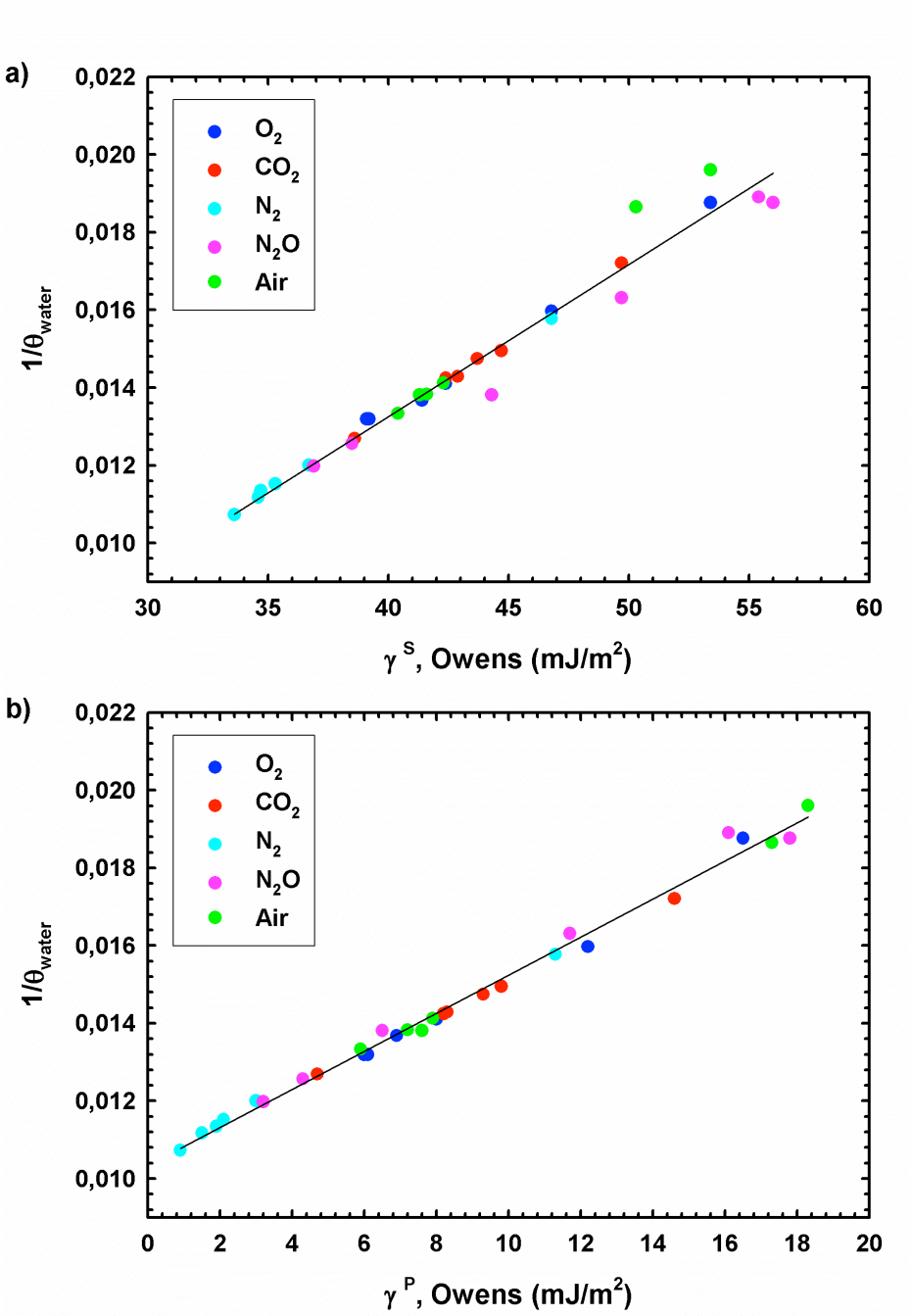

Figure 9. Linear relationship between (a) $1/\theta_{water}$ and γ^S; (b) $1/\theta_{water}$ and γ^P for plasma treated polypropylene according to the experimental parameters defined in Figure 8.

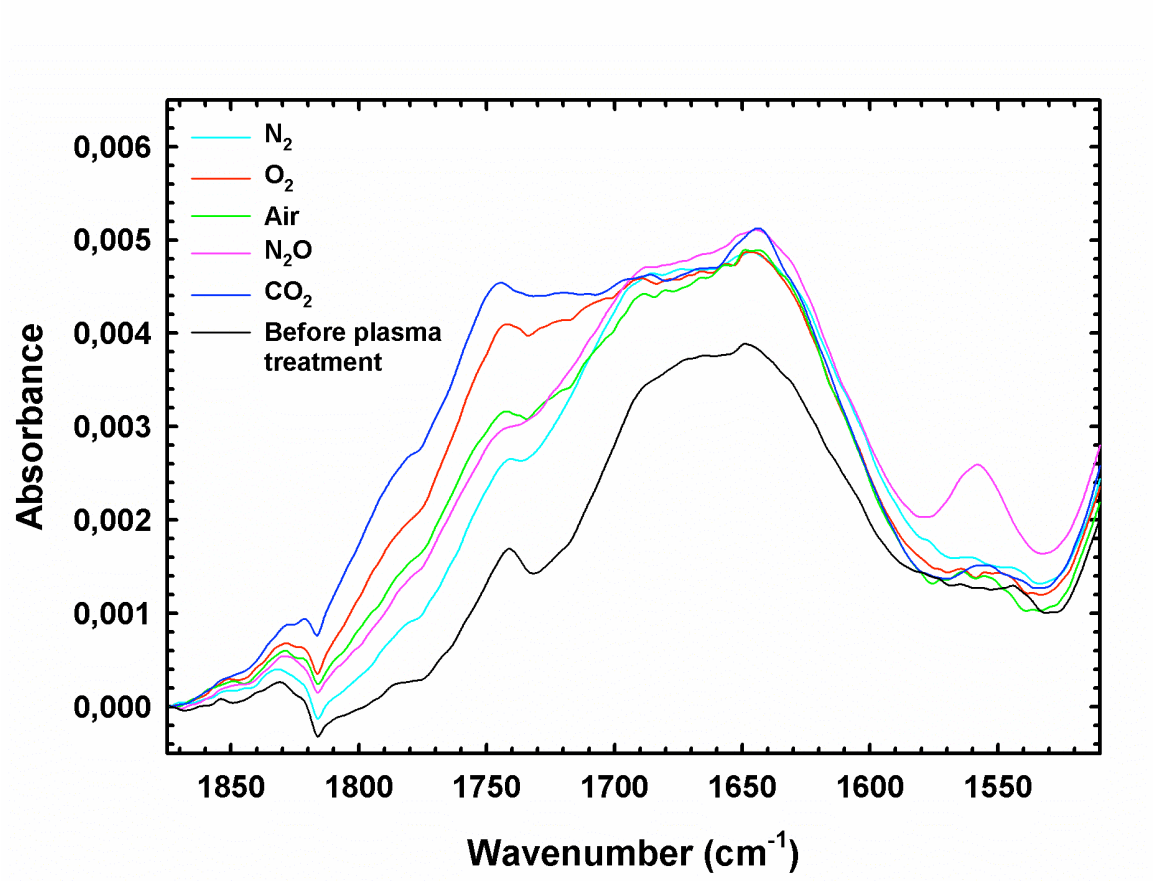

Figure 10. ATR-IR spectra of the carbonyl region (C=O stretching vibrations) for plasma treated polypropylene (see Table 1 for plasma treatment parameters).

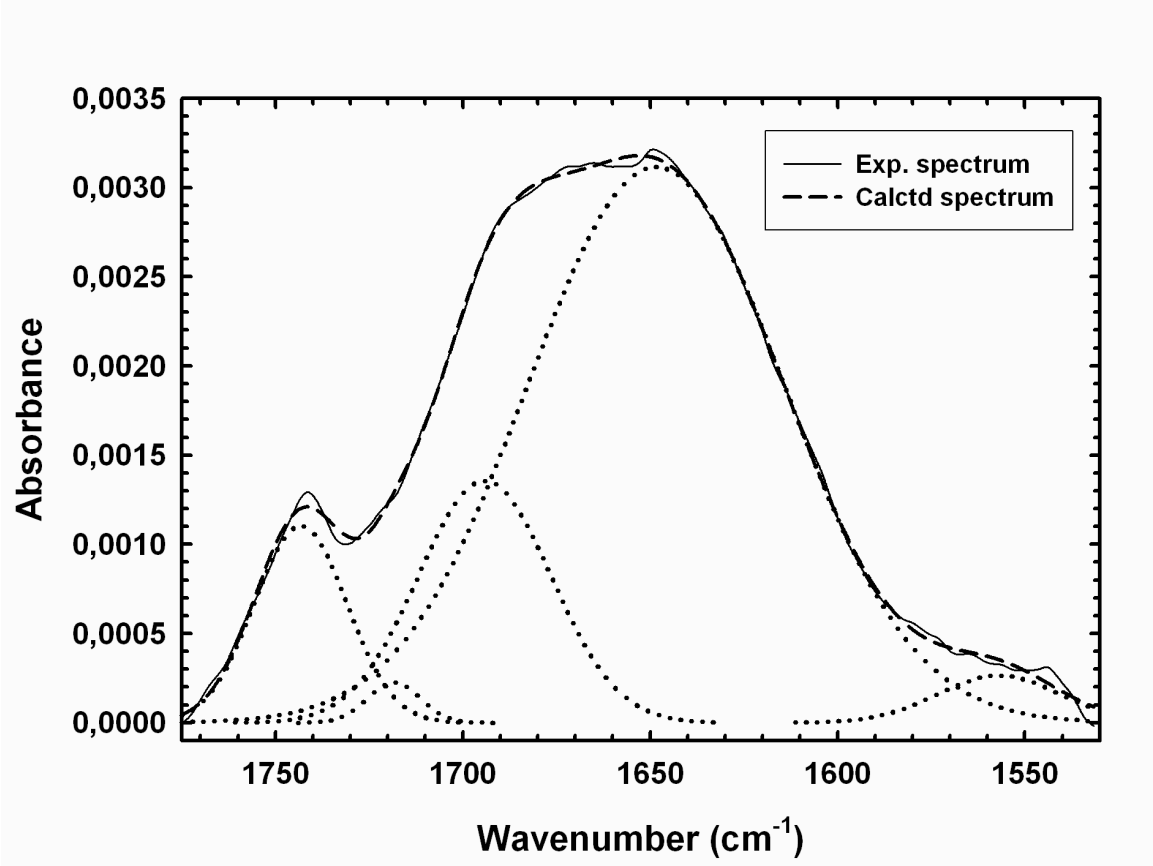

Figure 11. Decomposition of the ATR-IR spectrum recorded in the carbonyl region for polypropylene before plasma treatment.

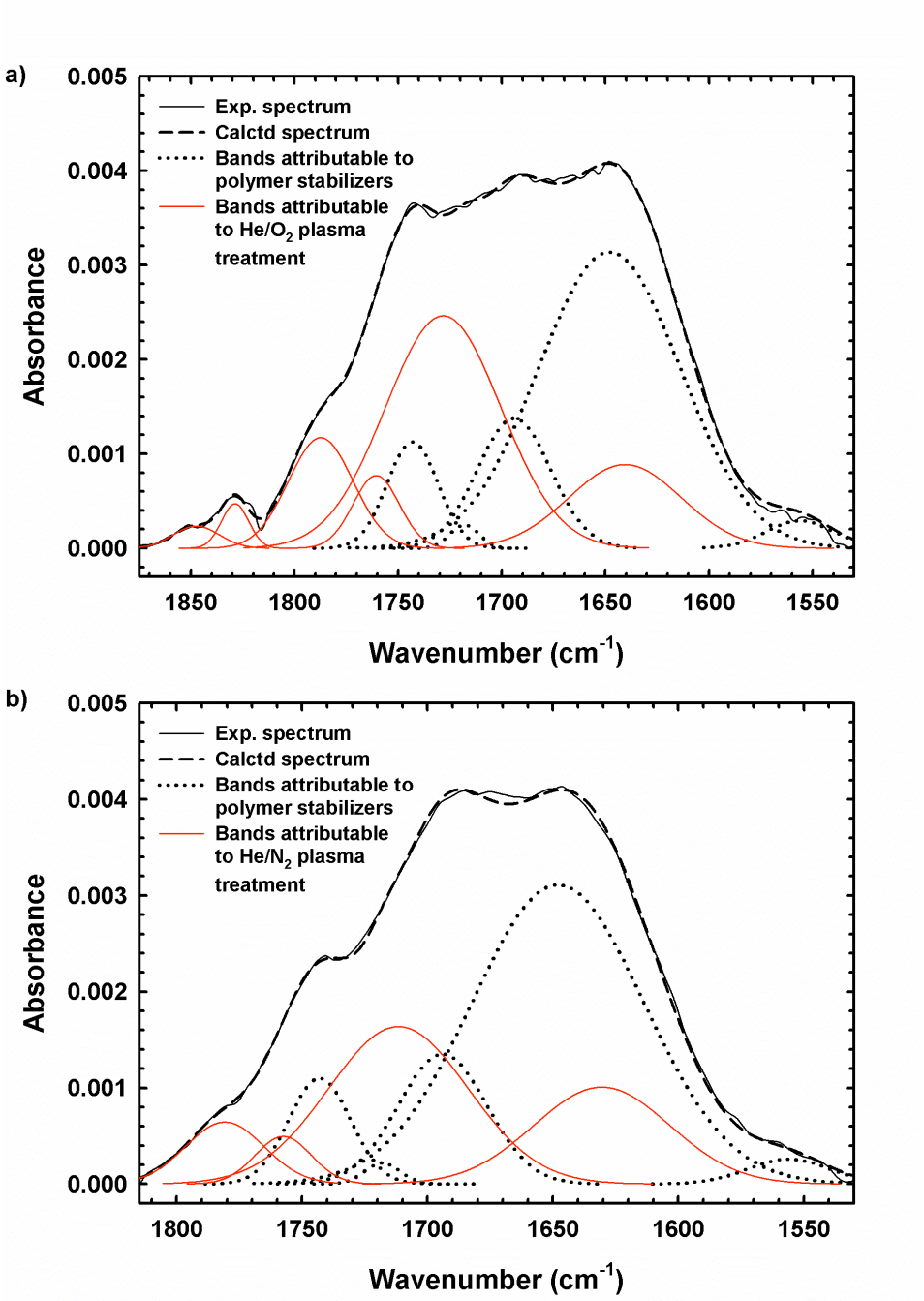

Figure 12. Decomposition of the ATR-IR spectra recorded in the carbonyl region for polypropylene following (a) He/O_2 ; (b) He/N_2 plasma treatments (see Table 1 for plasma treatment parameters).

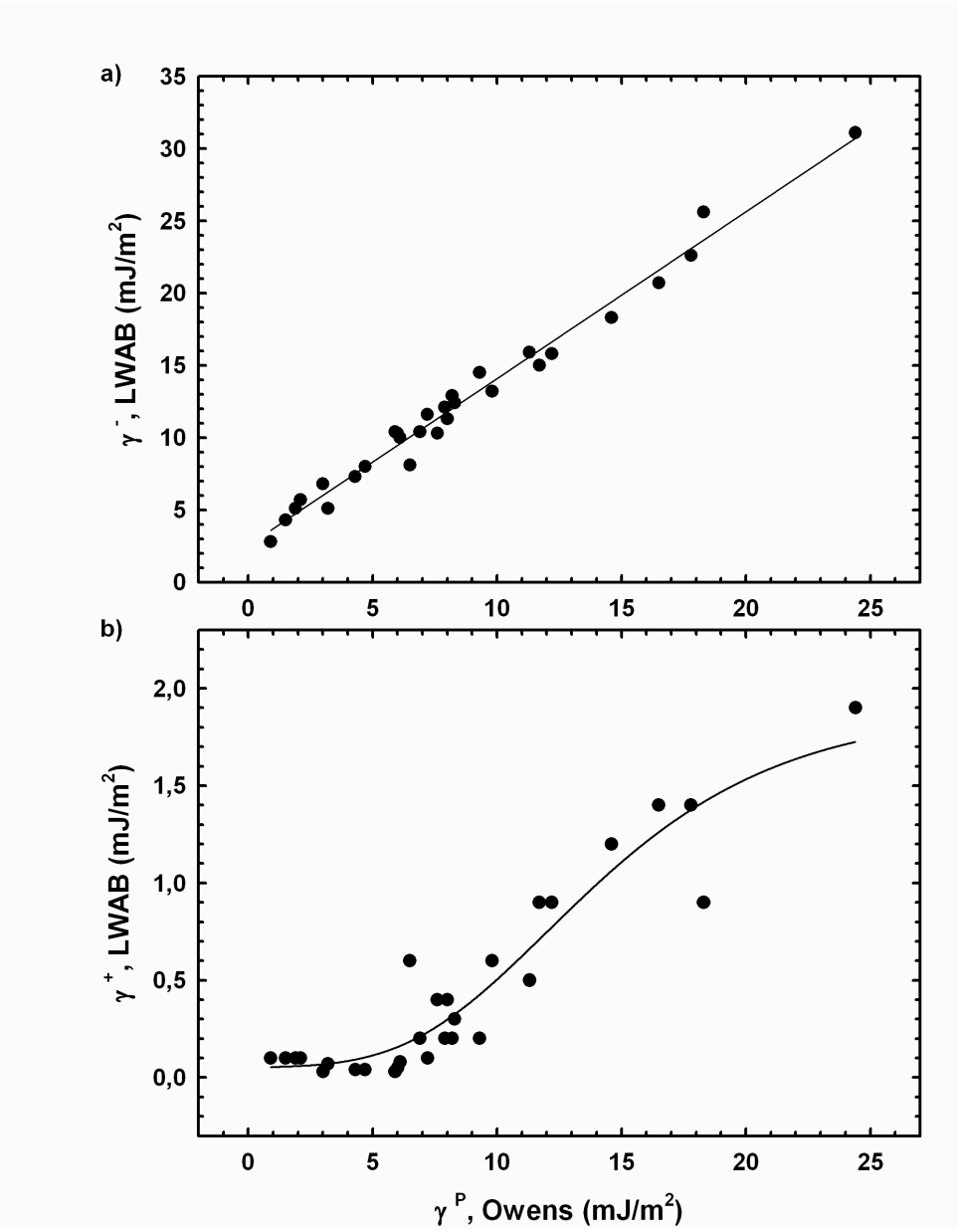

Figure 13. Relationship between (a) γ^- and γ^P; (b) γ^+ and γ^P calculated using Owens et al. and LWAB theories for polypropylene treated using the experimental plasma conditions defined in Figure 8.

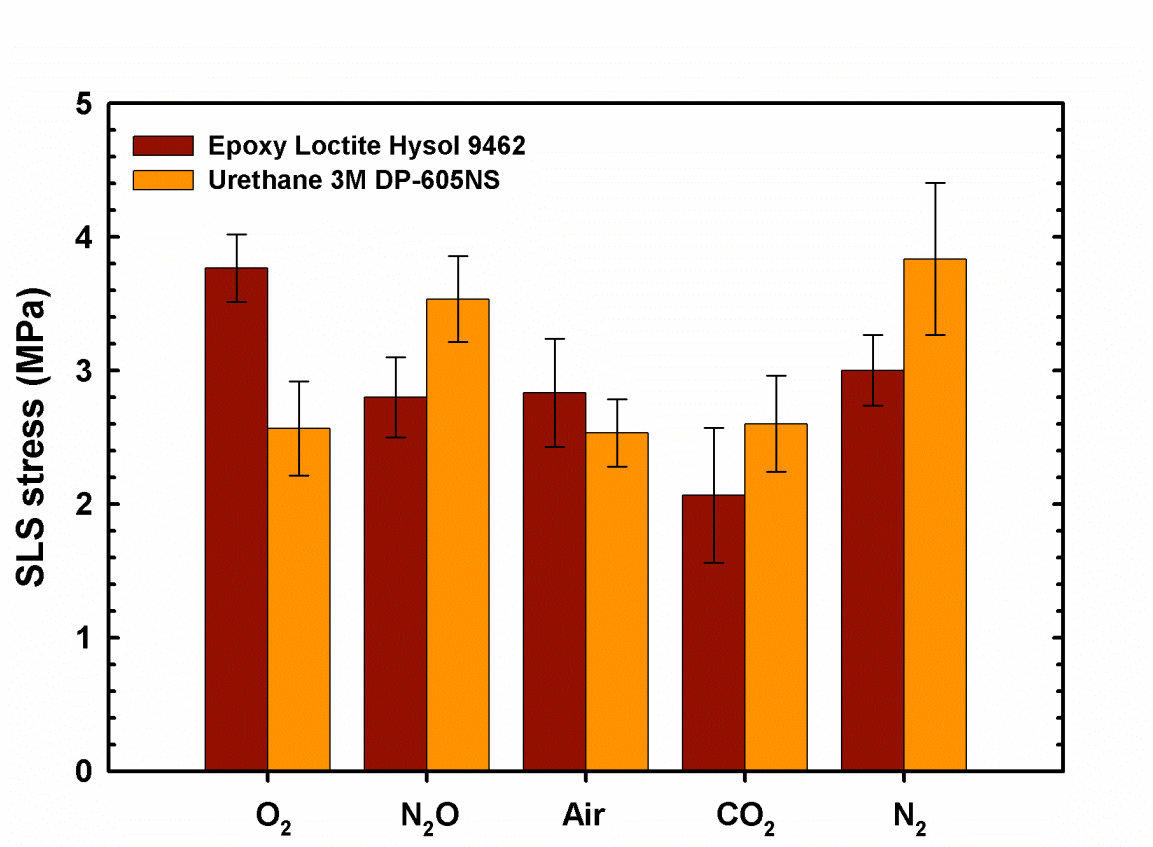

Figure 14. Single lap shear stress measured for aluminium-polypropylene hybrid assemblies as a function of the surface treatment of polypropylene and adhesive chemistry (see Table 1 for plasma treatment parameters).

Table 1. Optimised plasma treatment conditions using He 30 L/min as carrier gas and O_2, N_2O, Air, CO_2 and N_2 as secondary gases (1 pass, v = 300 cm/min, plasma-to-sample distance = 2 mm, plasma head model AH-250C).

Secondary gas	O_2	N_2O	Air	CO_2	N_2
Power (W)	150	150	150	150	60
Flow (mL/min)	300	100	200	50	350